Signatures of Indian Ocean Dipole and El Niño–Southern Oscillation events in sea level variations in the Bay of Bengal

S. G. Aparna,[1] J. P. McCreary,[2] D. Shankar,[1] and P. N. Vinayachandran[3]

Received 17 March 2012; revised 3 September 2012; accepted 4 September 2012; published 17 October 2012.

[1] We investigate the impact of the Indian Ocean Dipole (IOD) and El Niño and the Southern Oscillation (ENSO) on sea level variations in the North Indian Ocean during 1957–2008. Using tide-gauge and altimeter data, we show that IOD and ENSO leave characteristic signatures in the sea level anomalies (SLAs) in the Bay of Bengal. During a positive IOD event, negative SLAs are observed during April–December, with the SLAs decreasing continuously to a peak during September–November. During El Niño, negative SLAs are observed twice (April–December and November–July), with a relaxation between the two peaks. SLA signatures during negative IOD and La Niña events are much weaker. We use a linear, continuously stratified model of the Indian Ocean to simulate their sea level patterns of IOD and ENSO events. We then separate solutions into parts that correspond to specific processes: coastal alongshore winds, remote forcing from the equator via reflected Rossby waves, and direct forcing by interior winds within the bay. During pure IOD events, the SLAs are forced both from the equator and by direct wind forcing. During ENSO events, they are primarily equatorially forced, with only a minor contribution from direct wind forcing. Using a lead/lag covariance analysis between the Niño-3.4 SST index and Indian Ocean wind stress, we derive a composite wind field for a typical El Niño event: the resulting solution has two negative SLA peaks. The IOD and ENSO signatures are not evident off the west coast of India.

Citation: Aparna, S. G., J. P. McCreary, D. Shankar, and P. N. Vinayachandran (2012), Signatures of Indian Ocean Dipole and El Niño–Southern Oscillation events in sea level variations in the Bay of Bengal, *J. Geophys. Res.*, *117*, C10012, doi:10.1029/2012JC008055.

1. Introduction

[2] El Niño and the Southern Oscillation (ENSO) is known to have a global impact on climate [see, e.g., *Philander*, 1990]; in particular, the wind anomalies associated with ENSO extend to the Indian Ocean (IO) and affect the circulation in much of the basin [*Schott et al.*, 2009]. The Indian Ocean Dipole (IOD; also referred to as the Indian Ocean Zonal Mode, IOZM, or by the combinations, IODZM or IOZDM) was first described comprehensively by *Saji et al.* [1999], and subsequent work led to IOD and ENSO being identified as the two dominant modes of interannual climate variability in the IO. The impact of these two phenomena on the IO circulation, particularly in the Equatorial Indian Ocean (EIO), has since received considerable attention [*Schott et al.*, 2009].

[3] Although both ENSO and IOD are modes of IO climate variability, there is a distinct difference between their signatures over the IO. During ENSO, the signs of sea-surface temperature (SST) and sea-surface pressure (SSP) anomalies tend to be the same over the entire IO [*Klein et al.*, 1999; *Tozuka et al.*, 2008; *Schott et al.*, 2009; *Behera and Yamagata*, 2003; *Harrison and Larkin*, 1996], but these anomalies exhibit a dipole pattern during an IOD event. During a positive IOD event, SSP increases (decreases) and SST decreases (increases) over the eastern (western) tropical IO. As a result, easterly zonal wind anomalies occur during a positive IOD event [*Saji et al.*, 1999; *Webster et al.*, 1999; *Reverdin*, 1985; *Murtugudde et al.*, 1998, 2000; *Shankar*, 1998]. The dipole signature during an IOD event is seen in sea level too, with the level falling (rising) in the eastern (western) tropical IO [*Saji et al.*, 1999; *Webster et al.*, 1999].

[4] Differences between ENSO and IOD events extend to temporal variability. The IOD events are phase-locked to the seasonal cycle, with anomalies appearing during boreal summer and fall; in contrast, basin-wide anomalies associated with ENSO appear in the IO during winter and spring [*Vinayachandran et al.*, 2009]. During an IOD event, easterly wind anomalies are seen as the positive IOD phase sets in, and these anomalies continue during the rest of the event. Wind anomalies are of longer (shorter) duration of during an IOD (ENSO) event [*Rao et al.*, 2002a].

[5] Interannual variability is not restricted to the EIO, but extends into the North Indian Ocean (NIO) as well [*Clarke and Liu*, 1994; *Shankar*, 1998; *Shankar and Shetye*, 1999;

[1]CSIR National Institute of Oceanography, Dona Paula, India.
[2]SOEST, University of Hawai'i at Mānoa, Honolulu, Hawai'i, USA.
[3]Centre for Atmospheric and Oceanic Sciences, Indian Institute of Science, Bangalore, India.

Corresponding author: S. G. Aparna, CSIR National Institute of Oceanography, Dona Paula, Goa, 403004, India. (aparna@nio.org)

0148-0227/12/2012JC008055

Table 1. List of Pure Positive IOD, Pure El Niño, and Combined Events[a]

Positive IOD Events	El Niño Events	Combined Events
1961, 1967, 1983, 2007, 2008	**1957**–**58**, **1965**–**66**, 1976, 1969, **1986**–**87**, 1991–92 1993, 2002, 2004	1963, **1972**, 1977 **1982**, 1994, **1997** 2006

[a]Strong events are in bold font. The list of strong and weak ENSO events was obtained from the following sources: http://www.wrcc.dri.edu, Golden Gate Weather Service (http://www.ggweather.com), and *Trenberth* [1997]. El Niño events during 1957–1958, 1965–1966, 1976–1977, 1991–1992 are phase locked to the annual cycle and during 1968–1970, 1986–1987 extended for longer duration. The list of IOD events was obtained from *Berthot et al.* [2005], *Saji et al.* [2005], and *Hong et al.* [2008]. The strong and weak IOD events are defined based on *Berthot et al.* [2005] and DMI indices from the Web sites http://www.jamstec.go.jp/frcgc/research/d1/iod/sstdmi.txt and http://www.jamstec.go.jp/frcgc/research/d1/iod/DATA/dmi_HadISST.txt. There were some years when an ENSO event co-occurred with an IOD event. We divided these events into three categories: (a) pure IOD events, (b) pure ENSO events, and (c) co-occurring IOD and ENSO events (combined events). A pure IOD event is that which occurred in the absence of an ENSO event [*Rao et al.*, 2002a]. Following *Saji and Yamagata* [2003], we considered a positive (negative) IOD event that co-occurred with a La Nina (El Niño) a pure IOD event. A pure ENSO event was defined similarly. We considered the combined event to be strong only if both El Niño and positive IOD events were strong.

Han and Webster, 2002; *Singh*, 2002; *Rao et al.*, 2002b; *Srinivas et al.*, 2005; *Durand et al.*, 2011]. *Shankar* [1998] reported large negative sea level anomalies (SLAs) off the Indian east coast during 1961, one of the strongest positive IOD events on record. During an El Niño, negative SLAs are seen off the east coast [*Srinivas et al.*, 2005], and during a La Niña, positive SLAs [*Singh*, 2002].

[6] In the present study, we ask the following questions. First, does sea level variability, which is a better indicator of internal dynamics of the ocean than is SST, also exhibit distinct spatial and temporal patterns in the IO during IOD and ENSO events? We focus on sea level variability in the Bay of Bengal (BoB or bay), because it connects directly to the EIO through Kelvin-wave reflection at its eastern boundary [*Potemra et al.*, 1991; *McCreary et al.*, 1993, 1996]; furthermore, earlier studies [*Singh*, 2002; *Srinivas et al.*, 2005] suggest a weakening of the La Niña and El Niño signals on the west coast of India. Second, are the IOD and ENSO sea level signals clearly distinguishable in the BoB? In other words, can sea level anomalies there be used as a proxy for IOD and El Niño? Finally, how do these signatures change with intensity of the event, and how are they modified during "combined" events, that is, when both ENSO and IOD occur together?

[7] To answer these questions, we analyze and compare the sea level variability that occurs in the BoB during the ENSO, IOD, and combined events that occurred from 1958–2008 (see Table 1 for the list of events). We show that the sea level signals are so distinct in the BoB during ENSO and IOD events that they can be used to distinguish them. Model simulations are used to identify the processes responsible for the different responses for each type of event.

[8] We begin by showing that IOD and ENSO leave different signatures on the tide-gauge data from the east coast of India (Section 2.2). Tide-gauge data are available for a sufficiently long duration to cover many IOD and ENSO events, and, in particular, they capture the strong positive IOD event in 1961. The basin-wide signatures are described using altimeter data (Section 2.3), which are available from 1993 onwards. Following the description of these observed signals, we use a linear model to identify the processes that lead to the different signatures of these phenomena (Section 3). Section 4 concludes the paper.

2. Observations

2.1. Data

[9] We use monthly-mean sea level data for 1957–2008 at Chennai (Madras) and Visakhapatnam on the Indian east coast, obtained from the archives of the Permanent Service for Mean Sea Level (PSMSL), (Figure 1a). We use uncorrected sea level data for the analysis because the effect of atmospheric pressure on sea level at interannual time scales is not significant [*Ponte*, 1993; *Shankar et al.*, 2010]. The correlation between corrected and uncorrected sea level is 0.98 at both locations. The altimeter data are based on the gridded sea–level product from AVISO (Archiving, Validation, and Interpretation of Satellite Oceanographic data) for 1993–2008. The AVISO product merges data from several altimeters to produce a weekly SLA field on a $0.33^\circ \times 0.33^\circ$ Mercator projection grid [*Ducet et al.*, 2000].

2.2. Tide-Gauge Data

[10] A monthly climatology of sea level constructed from PSMSL data shows two maxima, a minor peak during May–June, and a major one during November, and a minimum during April at both Chennai and Visakhapatnam (Figure 1b). This monthly climatology is subtracted from the monthly sea level data to obtain monthly SLAs during 1957–2008 (Figure 1c). We use the data from these two locations for the analysis below.

2.2.1. Pure Positive IOD Events

[11] During 1961, a strong, pure positive IOD event (for definition, please see the caption of Table 1), negative SLAs were observed along the east coast of India during May–December (Figure 1c). SLAs were positive during January–March, but the positive IOD started in April and negative SLAs were seen in May. As the positive IOD matured, the negative SLAs increased in magnitude, peaking during October when the IOD event was also at its peak phase. Both the IOD and SLAs weakened during November, and by January 1962 positive SLAs were observed along the coast.

[12] The above SLA cycle is typical of pure positive IOD events, with negative SLAs following the IOD development-decay cycle. At the same time, the magnitude and timing of the SLAs are event-specific, depending on the intensity of the IOD event: The stronger the event, the higher the magnitude of the negative SLAs. For example, the SLA minima at Chennai was ~19 cm in October 1961 during a strong IOD event, ~14 cm in November 1967 during a moderate one, and negative SLAs were not observed at all during the weak 1983 event.

2.2.2. Pure El Niño Events

[13] During 1965–1966, a strong, pure El Niño event, negative SLAs were observed twice (Figure 1c). The El Niño event started in May 1965 and positive SLAs were observed at both Chennai and Visakhapatnam. Negative SLAs were first seen in July and the minimum occurred in November. Subsequently, the SLAs relaxed, sea level increased and positive SLAs were observed until January 1966. Thereafter, with El Niño in its mature phase, the SLAs turned negative

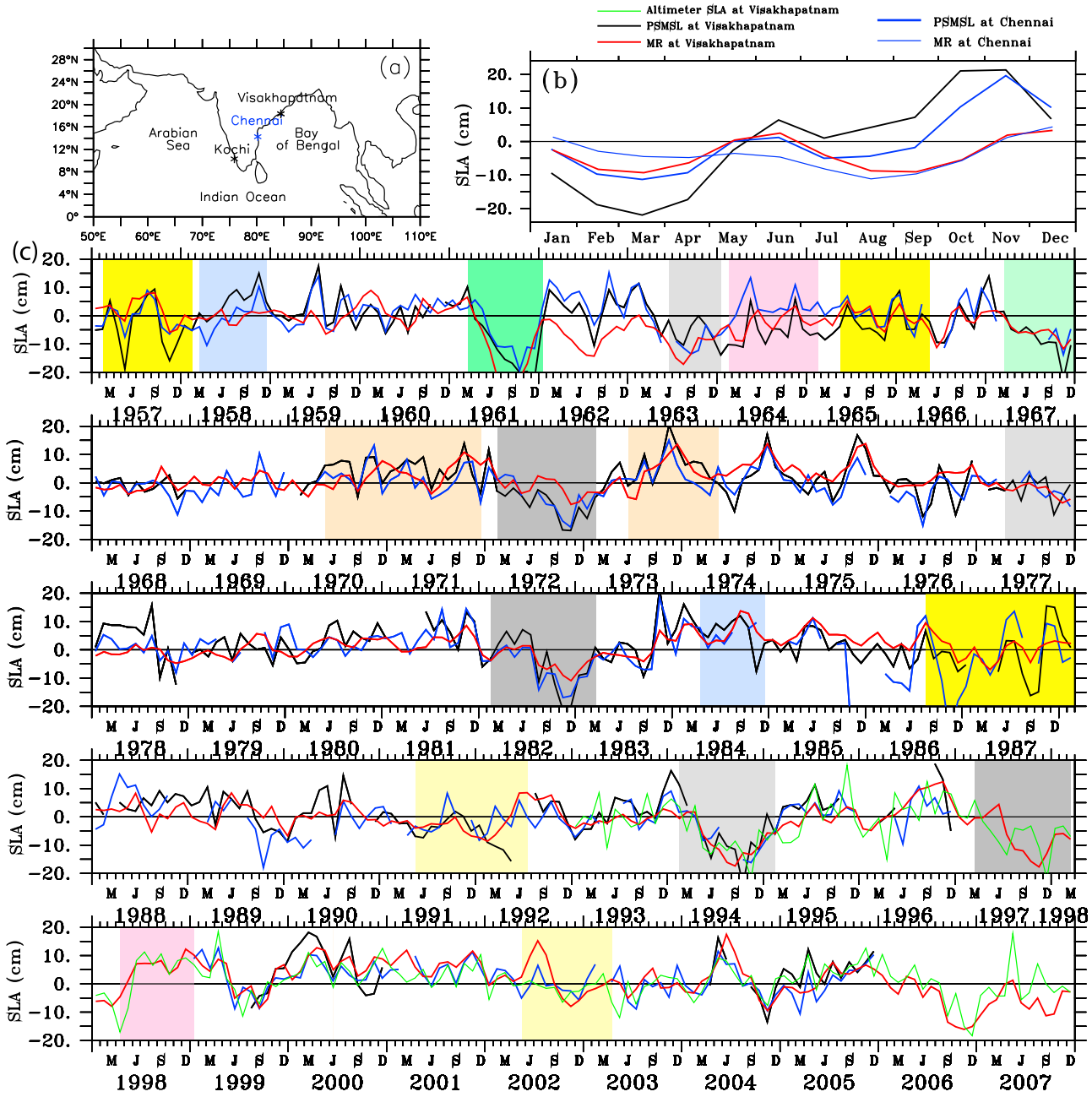

Figure 1. (a) Model basin north of the equator. (b) Comparison of model (MR) sea level monthly climatology (red) with PSMSL data at Visakhapatnam (black) and Chennai (blue). Thick (thin) lines are for the observations (model). (c) Monthly SLAs at Visakhapatnam (black) and Chennai (blue) during 1957–2007; the model SLA is shown only for Visakhapatnam (red) because the SLAs at Chennai were almost the same (unlike in the climatology). Altimeter SLAs (green) at Visakhapatnam are shown for 1993–2007. The strong (dark color) and moderate (light color) positive IOD and El Niño events are shown in background shades. Pure positive IOD events are in green shade, pure El Niño in yellow shade, and combined events (positive IOD and El Niño events) in grey shade. Pure negative IOD events are in light blue shade and pure La Niña events in ivory (cream) shade and combined events (negative IOD and La Niña events) are in pink shade. The correlation coefficients at Visakhapatnam and Chennai are 0.6 and 0.5, respectively. The regression coefficients a (intercept) and b (slope) at Visakhapatnam (Chennai) are 0.47 (−0.1) and 0.85 (0.7), respectively.

again. A second minimum in sea level occurred in March 1966. The negative SLAs relaxed again by April 1966 and the event decayed by June. A third peak in negative SLAs was seen during July, following the decay of the event.

[14] This SLA cycle is typical of pure El Niño events, with negative SLAs generally seen along the east coast of India a few months after the El Niño starts to develop in the Pacific Ocean. As the El Niño matures, the negative SLAs increase

in magnitude, attaining a peak sometime during April–December. This first minimum is followed by a relaxation of the negative SLAs, which even become positive during a few events. A second phase of negative SLAs is seen after a few months, typically during November–July. The second sea level minimum is followed by another relaxation of the negative SLAs as the El Niño diminishes, and a third sea level minimum occurs after its decay. Interestingly, two negative minima also characterize the SLAs in the Pacific Ocean during an El Niño [*Busalacchi et al.*, 1983; *Strub and James*, 2002; *Colas et al.*, 2008; *Xie et al.*, 2009], and they are often followed by a third [*Du et al.*, 2009].

[15] ENSO events are not as strictly phase-locked to the annual cycle as are the IOD events. The variability in the timing of El Niño in the Pacific implies that the time of occurrence of negative SLAs varies from event to event. Nevertheless, a majority of the events develop during March–July, peak during October–February, and diminish in the following spring. Examples of El Niño events that are and are not phase-locked to the annual cycle are given in Table 1. The complexity of the temporal variability of SLAs during an El Niño is evident in the long event of 1986–1988, which lasted for almost two years (Figure 1c). The two negative SLA peaks during October 1986 and April 1987 were followed by a strong negative SLA peak in September, and a weak fourth negative SLA peak was observed during February 1988. This long event of 1986–1988 can also be considered to be two successive El Niño events [*Clarke*, 2008], the first one from July 1986 to May 1987 followed by another from June 1987 to February 1988.

[16] The impact of El Niño is also dependent on the intensity of the event: the stronger the event, the higher the magnitude of the negative SLAs. For example, negative SLAs were greater than ∼10 cm at both Chennai and Visakhapatnam during the strong events in 1957–1958, 1965–1966, and 1986–1987, but negative SLAs were not observed during the weak event in 1969.

2.2.3. Combined Events

[17] El Niño events can co-occur with positive IOD events, and in that case, SLAs along the Indian east coast show signatures of both. In 1972, a strong combined event, negative SLAs were first observed during March (Figure 1c) with the onset of the positive IOD event. The negative SLAs strengthened during April and peaked in May. They relaxed during June–July, due to the developing phase of El Niño (its onset occurred during April), and as a result negative SLAs are not seen again until August. The second minimum in sea level occurred in November, when the positive IOD was at its peak. During all combined events, high negative anomalies are observed twice, a characteristic feature of El Niño. The second peak in the negative SLAs tends to occur late during the year, a signature of the phase-locked positive IOD event.

[18] Negative SLAs are higher in magnitude during strong combined events like 1972 and 1982 than they are during moderate combined events like 1963 and 1977. The combined events are more complex, however, owing to the possibility of a strong (weak) IOD co-occurring with a weak (strong) El Niño. During 1994, a moderate combined event, negative SLAs greater than 20 cm were observed owing to the strong positive IOD that co-occurred with a moderate El Niño. The strongest combined event occurred during 1997, but, unfortunately, PSMSL data were not available at this time at Visakhapatnam and Chennai. Altimeter data, however, were available during this event.

2.2.4. Negative IOD and La Niña Events

[19] The signatures of negative IOD and La Niña events, although seen in the observations, are much weaker than the signatures of the positive IOD and El Niño events. During negative IOD events, positive SLAs have a single peak during September–December, the month of occurrence depending on the time of the peak phase of the event. For example, during the 1958 and 1984 pure negative IOD events (Figure 1c), a peak is observed in positive SLAs during November 1958 and September 1984. During both events, however, a small bump in SLAs is observed during June–July.

[20] La Niña events, with two positive SLA peaks, mirror the El Niño events. For example, two SLA peaks are observed during the pure La Niña event of 1973–1974 (July and October) (Figure 1c). The 1970–1971 La Niña event is a long event and can be considered as two successive events (similar to the 1986–1988 El Niño events); positive SLAs are observed June and November 1970 (first part of the event) and during May and October 1971 (second part of the event).

[21] Two positive SLA peaks, with a relaxation between them, are observed during combined events. For example, during the 1964 combined event, two peaks are observed during May and November. During 1998–1999, PSMSL data are not available, but two peaks are observed in model and altimeter SLAs (Figure 1c).

2.3. Altimeter Data

[22] The distinct signatures of El Niño and positive IOD events in the tide-gauge data are not confined to the coast of India. Altimeter data show that they extend across the BoB.

[23] The only pure positive IOD events during the altimeter period occurred during 2007 and 2008. Unfortunately, both were moderate events and were unusual owing to the co-occurrence of positive IOD and La Niña. During September 2007, negative SLAs were observed in the bay (Figure 2). During 2007 (2008) negative SLAs were observed in the bay during June–November (June–August).

[24] The only pure El Niño event during the altimeter period occurred in 2002–2003, and it was a weak-to-moderate event. It started in May 2002 and ended in March 2003. Negative SLAs were observed in the bay during September–November. They relaxed during December 2002 and January 2003 (Figure 2), at which time positive SLAs were observed along the eastern and northern boundaries of the bay. From February 2003, sea level began to decrease again, and negative SLAs were observed for the second time during February–April 2003.

[25] The three combined (positive IOD plus El Niño) events that occurred during the altimeter period were moderate events in 1994 and 2006 and the strong event in 1997. Negative SLAs were observed in the bay twice during 1997, first during February–April and again during July–December (Figure 2); a relaxation in the negative SLAs occurred over parts of the bay during May–June.

[26] Negative IOD and La Niña events also have characteristic SLA patterns in the bay. As for the tide-gauge records along the east coast of India, however, signatures of negative IOD and La Niña are weaker in the rest of the BoB compared to positive IOD and El Niño events.

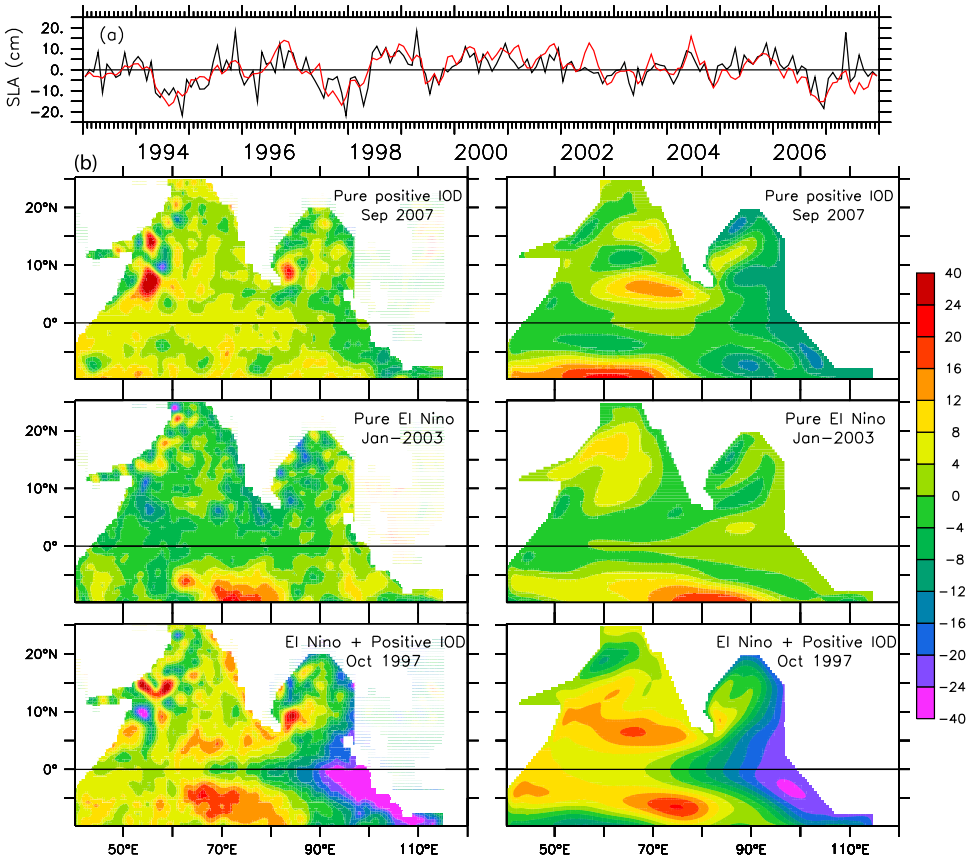

Figure 2. (a) Comparison of altimeter SLA (black) and Solution MR (red) at Visakhapatnam. (b) Comparison of (left) altimeter SLA with (right) model MR SLAs (cm) during (top) a pure positive IOD event, (middle) a pure El Niño event, and (bottom) a combined event.

[27] Despite the obvious problem of not covering an adequate number of events, the altimeter data confirm the distinct signatures of El Niño and positive IOD events along the Indian east coast and show that these differences extend across the BoB. Together, the two sea level data sets point to a distinct difference in the imprint of these two climate modes on the BoB.

3. Dynamics

[28] The SLA differences between IOD and ENSO must be driven primarily by differences in the wind forcing. To explore this idea, we obtain and analyze solutions to a linear, continuously stratified (LCS) model. We begin with a brief description of the ocean model, our experimental design, and analysis techniques; a detailed description of the model can be found in Appendix A. We then report solutions that illustrate the responses to IOD, ENSO, and combined events.

3.1. Ocean Model

[29] The equations of motion of the LCS model are linearized about a state of rest, with a background Brünt-Vaïsäla frequency, $N_b(z)$, and the ocean bottom is assumed to be flat. With these restrictions, solutions can be represented as expansions in vertical modes (barotropic and baroclinic) of the system. The choice of the density profile is the same as that used by *Moore and McCreary* [1990]. The first 10 baroclinic modes are summed to obtain solutions, the number of modes is based on earlier studies [*McCreary et al.*, 1996; *Shankar et al.*, 2010]; however, most of the sea level response is captured by the first two baroclinic modes. Solutions are found for a realistic basin geometry north of 29°S, with continental boundaries lying roughly along the 200 m isobath. The basin north of the equator is shown in Figure 1a; the full basin is shown in *Shankar et al.* [2010] and *McCreary et al.* [1993].

[30] The model ocean is forced by monthly-mean winds from the National Center for Environmental Prediction / National Center for Atmospheric Research (NCEP/NCAR) monthly reanalysis [*Kalnay et al.*, 1996]. We multiply the NCEP/NCAR winds with a taper function, which has a maximum value of 1.4 at the equator and decays to 1 within 10° latitude. We adopted these modifications by comparing the QuikSCAT and NCEP/NCAR climatological monthly wind data. It is consistent with the conclusions off *Chelton and Frielich* [2005], who showed that the root-mean square differences between NCEP and QuikSCAT winds during 2000 and 2002 are greater near the EIO compared to the NIO and south IO.

[31] Our main run (MR) is the solution obtained by applying the usual closed, no-slip condition at the continental boundaries. It captures all the major features of sea level variability in the NIO. Although the model climatology of sea level is weaker than observed (Figure 1b), the model

SLAs compare well with the PSMSL (Figure 1c) and altimeter (Figure 2) SLAs. Model climatological sea level compared well with observations in the simulations of *McCreary et al.* [1996], the likely reason for the weaker climatology in our simulations is the use of a weaker wind forcing: They used the wind-stress climatology of *Hellerman and Rosenstein* [1983], compared to which NCEP/NCAR winds are weaker [*Josey et al.*, 2002].

[32] We also obtained three "process" solutions that isolate the contributions of three forcing mechanisms: *i*) Rossby waves generated by the reflection of equatorially-trapped Kelvin waves at the Sumatra coast, *ii*) forcing by coastal winds along the perimeter of the bay, and *iii*) direct forcing by winds in the interior ocean. Similar separations have been carried out earlier for the entire IO [*Shankar et al.*, 2010], for the bay [*Shankar et al.*, 1996; *McCreary et al.*, 1996], and for the monsoon currents [*Shankar et al.*, 2002]. The process solutions are determined from the MR and two test solutions, TS1 and TS2, as follows. Solution TS1 differs from MR only in that it includes an equatorial damper (described in Appendix A) that filters out the effect of equatorial forcing on the bay. The difference, MR – TS1 (Solution EQ), then illustrates the effects of remote forcing only by the reflection of equatorial Kelvin waves from the eastern boundary of the basin (Sumatra). Solution TS2 applies special boundary conditions (equations (A5)) along continental boundaries of the NIO, filtering out the effect of alongshore winds and therefore of the coastal Kelvin waves generated by these winds. The difference, MR – TS2 (Solution CST), then illustrates the effect of alongshore winds. The third process solution, defined by MR – EQ – CST (Solution INT), eliminates effects of forcing from the equator and by alongshore winds, and hence quantifies the effects of direct forcing by winds in the interior ocean (Ekman pumping).

3.2. Pure Positive IOD Events

[33] During 1961, positive SLAs occur in the MR over most of the bay during January–March (Figure 3), but there is a cyclonic circulation around a relative low in sea level in the central bay. By April, when negative SLAs are seen in the eastern bay, the positive SLAs shift westward owing to Rossby-wave radiation, leading to an anticyclonic circulation around a sea level high. The negative SLAs strengthen and spread westward during May–October, narrowing the sea level high and intensifying the anticyclonic circulation. The negative SLAs peak during October, at which time they cover a large fraction of the bay, and positive SLAs are restricted to the southwestern bay. The negative SLAs weaken during November and are replaced by positive SLAs in the eastern bay in December.

[34] Solution EQ, which contains the reflected Rossby wave at the eastern boundary of the EIO, is essentially driven by the sea level signal in the eastern EIO (EEIO; Figure 3). The positive (negative) SLAs in the eastern bay are driven by westerly (easterly) wind anomalies over the EIO during January–February (March–October). The anomalous easterlies weaken the eastward Wyrtki jets [*Wyrtki*, 1971] in the EIO [*Reverdin*, 1985] and the associated negative SLAs propagate into the bay. In contrast to Solution EQ, which has a strong response in the eastern bay, Solution INT is strongest in the southwestern basin, where Ekman pumping is particularly strong (Figure 3). Positive Ekman pumping forces the weak negative SLAs in this region during January–April and negative Ekman pumping forces the strong positive SLAs there during May–December. Solution CST (figure not shown) is negligible in comparison to Solutions EQ and INT. Therefore, Solution EQ forces the negative SLAs in the MR and Solution INT the positive SLAs in the southwestern bay, which are out of phase with the rest of the basin. This pattern of sea level variability repeats during other positive IOD events.

3.3. El Niño Events

[35] Here, we first describe the sea level variability in the bay during the pure El Niño event of 1965–1966, followed by a discussion of a solution forced by composite ENSO winds. We conclude by noting the cause of the multiple sea level peaks that occur during ENSO.

3.3.1. The 1965–1966 El Niño

[36] The El Niño event of 1965–1966 started in May 1965. At that time, a cyclonic circulation seen in the MR is associated with positive SLAs along the perimeter of the bay (figure not shown). The cyclonic flow weakens by August, when negative SLAs are seen in the eastern bay (Figure 4). These negative SLAs strengthen and spread westward into the bay owing to Rossby wave radiation, peak in October (first minimum), and relax during December. The positive SLAs that replace them in the eastern bay also spread westward and are, in turn, replaced by negative SLAs in February 1966. As in the tide-gauge data, another peak in negative SLAs (the second minimum) occurs in March along the east coast of India (Figure 1c). This coastal minimum is followed first by a relaxation of the negative SLAs and then by a third minimum (July 1966), which occurs after the decay of the El Niño event in June 1966.

[37] As for a positive IOD event, Solution EQ for a pure El Niño event is also driven by the winds over the EEIO (east of 60°E). The positive (negative) SLAs in the eastern bay are driven by westerly (easterly) wind anomalies over the EIO during May–June 1965 (September–November 1965 and April–June 1966). The relaxation between the first and second minima in sea level is clearly due to Solution EQ. Solution INT makes only a weak contribution to the SLAs over most of the bay. As for a positive IOD event, its impact is stronger in the southwestern bay in comparison to the rest of the basin but the response during the pure El Niño event is weaker. The weak relaxation in negative SLAs at the coast between the second and third minima is, however, due to weak cyclonic Ekman pumping over the western bay. This coastal SLA response due to Solution INT exists during most of the year, but can overwhelm Solution EQ only when the latter weakens in this region. Solution CST is always negligible.

[38] Unlike for the positive IOD events, Solution EQ dominates the response during a pure El Niño event. This pattern of sea level variability repeats during other pure El Niño events, but there are more differences among these events compared to the pure IOD events owing to the greater variability in the EIO winds during an El Niño (Figures 3 and 4).

3.3.2. Composite El Niño

[39] In spite of the relative weakness of the pure El Niño signature, it stands out even in a composite analysis. The larger number of pure El Niño events in comparison to pure positive IOD events makes it possible to make a composite of the former but not of the latter. Although a similar variation in

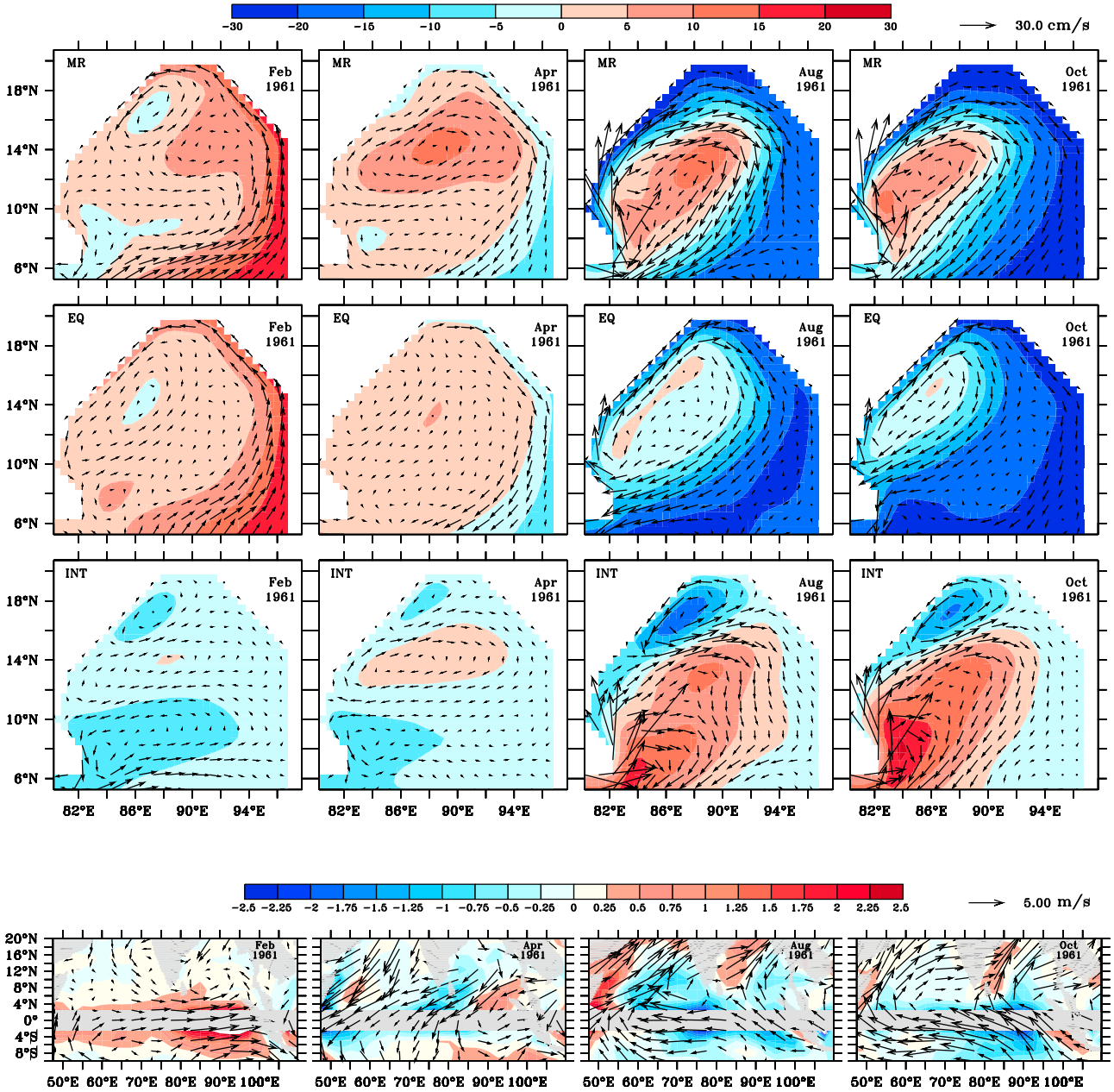

Figure 3. (top) Model MR monthly SLAs (cm) and surface currents during 1961, a strong, pure positive IOD event (top row). SLAs (color fill) and surface currents (vectors) are shown for Solution EQ (second row) and Solution INT (third row). (bottom) Ekman pumping anomalies (cm s^{-1}) and surface wind anomalies.

SLAs in the bay occurs during all pure El Niño events, the magnitude and timing of the peaks in negative SLAs vary considerably from event to event. Therefore, it is not possible to calculate a composite of pure El Niño years by averaging SLAs for each month during these events: the start, duration, and end of the each individual event are different, and the signature of El Niño in sea level variations in the bay is quite sensitive to the timing. We therefore used covariance analysis to compute a composite of the wind stress field during an El Niño year.

[40] Let $W_j(x, y)$ be the anomalous wind stress field at each point (x, y) in the domain, where j is a month index. (Variable W_j includes anomalies for both τ_x and τ_y, which are calculated by removing the climatological annual cycle of τ_x and τ_y at every grid point.) Also let E_j be the Niño-3.4 SST-anomaly index. Then, the composite wind stress field for both x and y components, is defined by

$$\mathcal{W}_i(x,y) = \frac{\mathrm{cov}\left(E_j', W_{j+i}\right)}{\mathrm{cov}\left(E_j', E_j'\right)}, \qquad (1)$$

where E_j' is the average of E_j from November(0) to January(1), and 0 and 1 represent the developing and decaying years of the El Niño event. Index i represents the lead/lag in months with respect to the peak of the El Niño: $i = 0$ is the

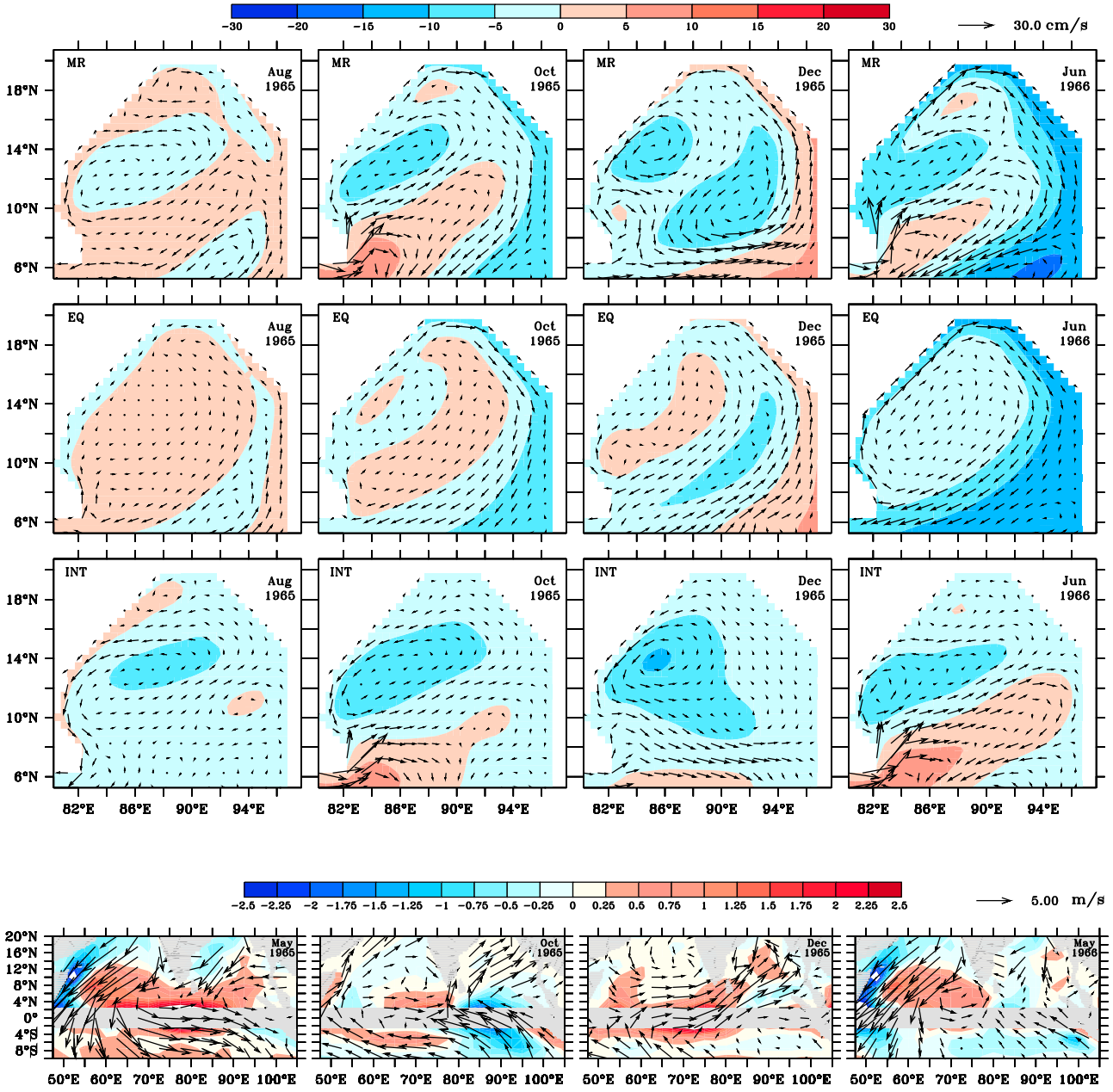

Figure 4. Same as Figure 3, but for the pure El Niño event during 1965–1966.

month during which El Niño is at its peak and the lead (lag) indicates that the wind field W_j leads (lags) the Nino-3.4 SST index E_j'. According to (1), $\mathcal{W}_i$ represents an average of wind anomalies during all the El Niño events, whether weak, moderate, or strong. We therefore multiply $\mathcal{W}_i$ by a factor to compensate for the varying strength of the events, and forced the LCS model with this anomalous wind stress.

[41] Figure 5 shows the resulting sea level variation during a composite El Niño event. The El Niño peaks at $i = 0$, which, in general, corresponds to December because most of the events peak during November(0)–January(1). During the developing year (0), negative SLAs are first observed along the perimeter of the bay during February ($i = -10$; figure not shown). These negative SLAs spread westward as Rossby waves into the bay and peak in May ($i = -7$). The negative SLAs relax during June–July ($i = -6, -5$) and reverse sign over most of the bay. During these months, the composite wind field $\mathcal{W}_i$ is westerly over the EIO. Negative SLAs occur again during August ($i = -4$; figure not shown) and strengthen and spread westward until December ($i = 0$). Following the El Niño peak, the negative SLAs weaken, but continue to spread westward across the bay until the signal decays in April ($i = 4$; figure not shown) of the decaying year (1). The composite El Niño SLAs are driven mainly by Solution EQ; Solution INT makes a contribution in the

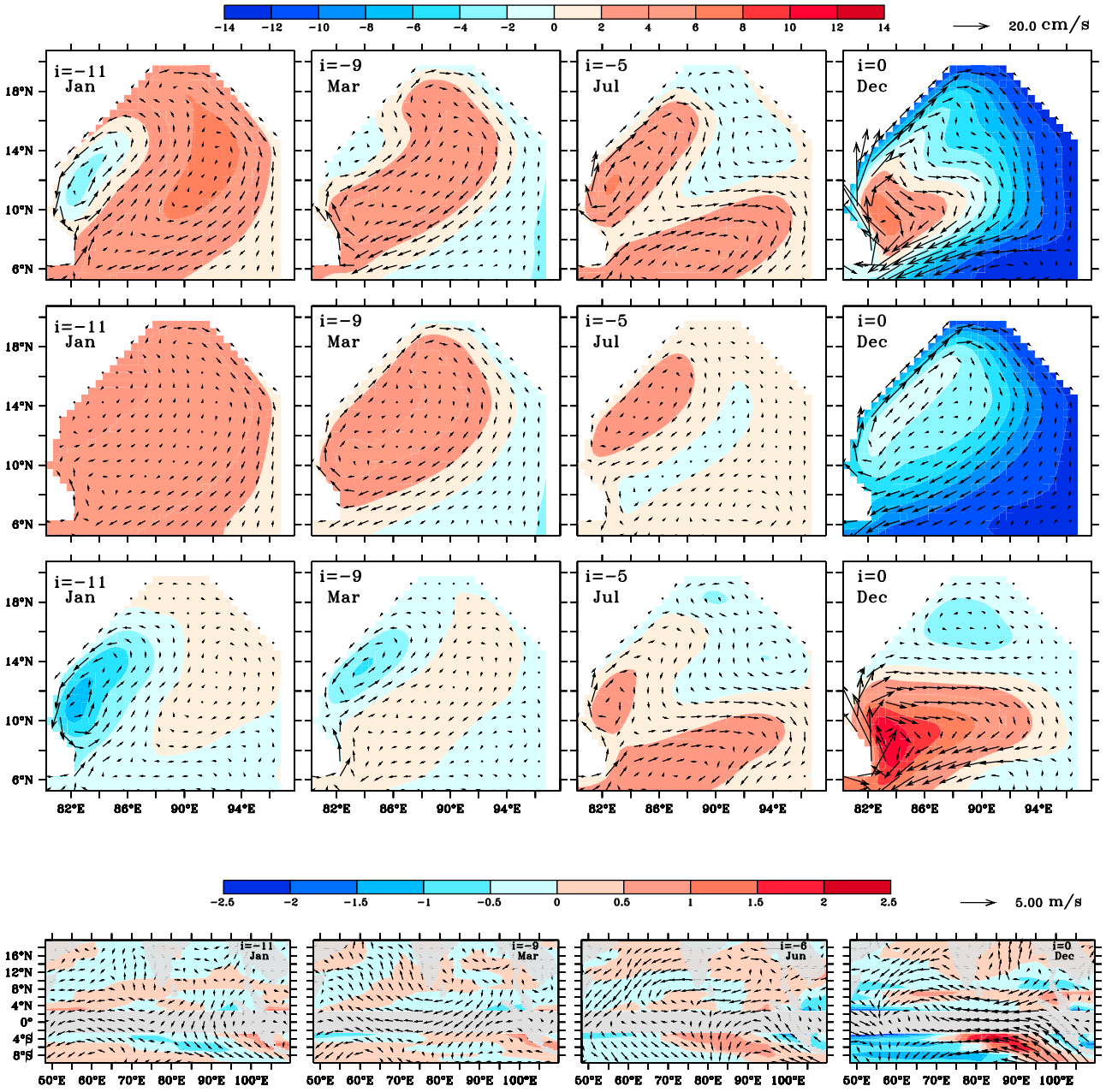

Figure 5. Same as Figure 3, but for the composite El Niño event. This composite El Niño event may be classified as a moderate-to-strong event.

southwestern bay, where it forces the positive SLAs and along the east coast of India (Figure 5).

3.3.3. Cause of Multiple SLA Peaks

[42] The reason for the multiple SLA peaks during El Niño events lies in the equatorial wind field. Studies show that a strong, well-defined, single Walker cell exists over the EIO during summer and autumn in pure positive IOD years such as 1961 and 1967 [*Ashok et al.*, 2003]. This feature of a positive IOD event is consistent with strongly divergent surface easterly winds over the EIO. In contrast, multiple Walker cells are seen over the EIO during El Niño years [*Ashok et al.*, 2003], weakening the surface easterly wind anomalies, which implies a weaker SLA response in the EIO and the bay. The multiplicity of Walker cells also leads to the reversal in wind anomalies over the EIO and the relaxation in negative SLAs in the bay during a pure El Niño event.

3.4. Combined Events

[43] To show the signatures of combined events in sea level variability, we describe the sea level variability in the bay during 1972–1973, a strong El Niño and strong IOD event. A similar pattern is observed in all combined events.

[44] Positive SLAs are seen in the MR during January–February 1972. Negative SLAs appear in the eastern bay during March when the positive IOD sets in, and they peak in May (Figure 6). The El Niño starts in April and positive SLAs, which appear in June, are seen almost everywhere in the bay by July. Negative SLAs develop in the eastern bay

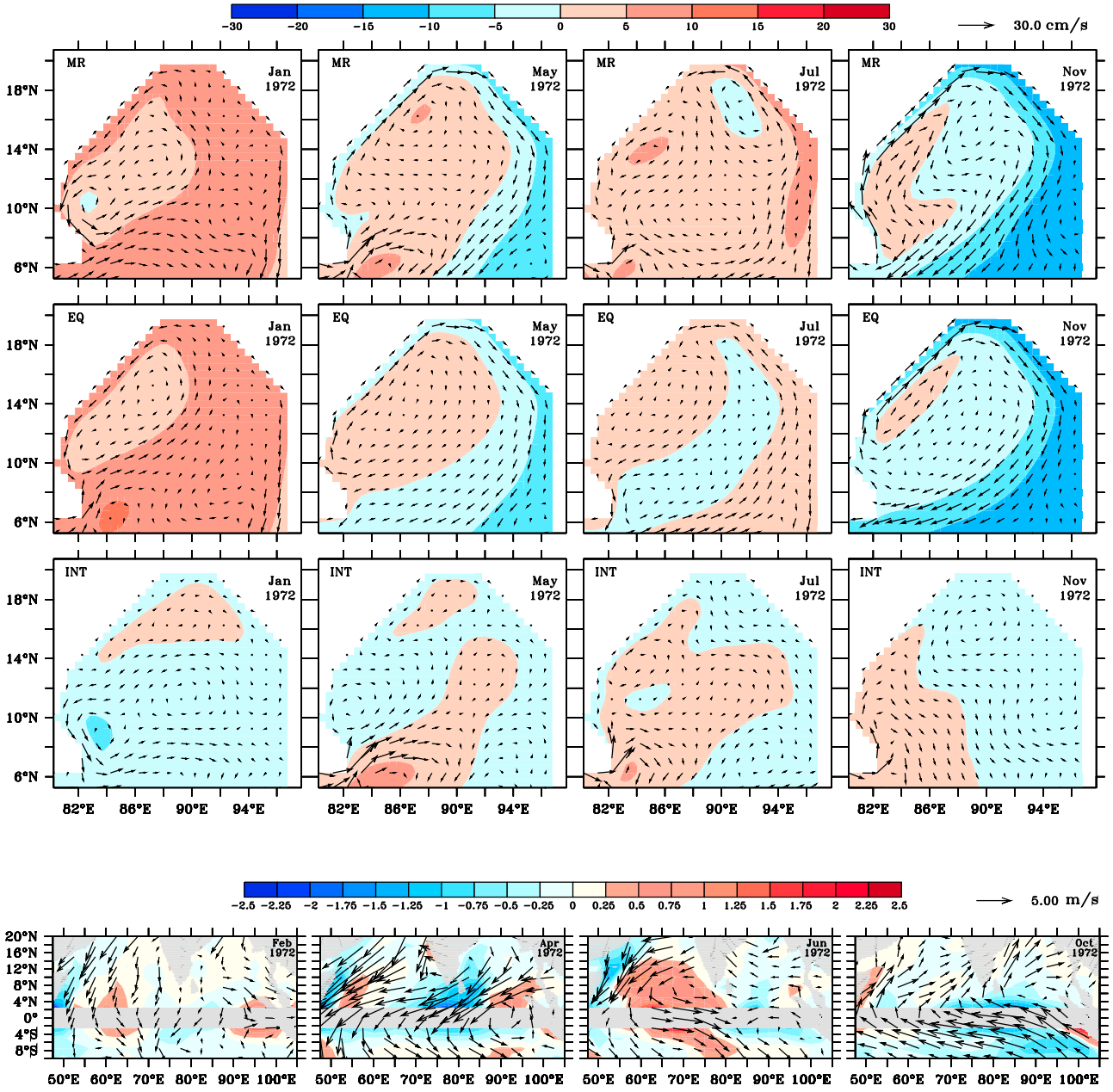

Figure 6. Same as Figure 3, but for the combined event during 1972.

again during August and strengthen throughout September–November, when they spread westward into the basin owing to Rossby-wave radiation. The negative SLAs peak in November, when the IOD and El Niño events are in their mature phase. The negative SLAs diminish thereafter, but they persist until March 1973 owing to the El Niño.

[45] Solution EQ dominates during this combined event. Indeed, its response is essentially the same as in MR, the only significant differences restricted to the southwestern bay. Positive SLAs, which occur between the two negative SLA peaks in May and November, are due to westerly wind anomalies over the EIO during June–July. The easterly wind anomalies are stronger in October because the El Niño and positive IOD are in phase at this time, leading to the stronger negative SLA peak in November; this second peak in 1997 event was also reported by *Chambers et al.* [1999] and was shown by *Yu* [2003] to be forced remotely from the EIO.

[46] In general, during a combined event, the sea level variability shows characteristics of both positive IOD and El Niño. The timing and phase of El Niño is important for deciding the strength of the SLAs because the positive IOD is locked to the seasonal cycle. An example is the strong combined event of 1997, during which the magnitude of the first peak in negative SLAs is not as high as during the weaker 1972 event because the onset of positive IOD occurred only during May–June 1997. This delay ensured that the phases of the positive IOD and El Niño were not synchronous, leading to strong negative SLAs being observed only during November (second minimum).

3.5. The Southwestern Bay of Bengal

[47] During both positive IOD and El Niño events, the southwestern bay is out of phase with the rest of the basin. Negative SLAs are a characteristic feature of these events, but the SLAs tend to be positive in the southwestern bay. This region is where the Bay-of-Bengal Dome and Sri-Lanka Dome form during the summer monsoon [*Vinayachandran and Yamagata*, 1998]. (The nomenclature indicates a cyclonic circulation with the thermocline shallowing or "doming.") The positive SLAs imply an anomalous deepening of the thermocline. Positive SLAs in the southwestern bay have been reported earlier: *Vinayachandran et al.* [2002] reported positive SLAs in the southwestern bay during the 1994 and 1997 combined events, *Vinayachandran and Mathew* [2003] reported the positive SLAs in the BoB dome region during 1997 event, and *Thompson et al.* [2006] reported positive SLAs during all IOD events except 1967. The anomalies are stronger during a positive IOD event compared to El Niño, but the key process in both cases is Ekman pumping (Solution INT), identified by *Vinayachandran and Yamagata* [1998] as the driving mechanism for both domes. The anticyclonic Ekman pumping anomaly in this region is due to equatorial easterly anomalies, just as the normally observed cyclonic Ekman pumping in the region is due to westerly winds over the EIO. This anticyclonic circulation in bay during positive IOD events is observed even at sub-surface levels (37.5 m) [*Rao et al.*, 2002a].

4. Summary and Discussion

[48] Prior studies have discussed the impact of the IOD and ENSO modes on NIO sea level variability [*Clarke and Liu*, 1994; *Han and Webster*, 2002; *Singh*, 2002; *Srinivas et al.*, 2005], showing that negative SLAs are prominent along the east coast of India during positive IOD events [*Han and Webster*, 2002; *Srinivas et al.*, 2005], but they did not distinguish between the two modes. In this study, we have shown that IOD and ENSO not only influence sea level variability in the BoB, but leave distinct signatures that can be used to characterize these events.

[49] Positive IOD events are characterized by a monotonic decrease in sea level (increasingly negative SLAs) along the east coast of India during the year; the phase-locking of this event to the seasonal cycle ensures that the negative SLAs terminate abruptly following their peak in October–November. During El Niño, negative SLAs tend to be weaker and occur, with an abrupt relaxation between the two peaks; on occasions, the SLA can even reverse sign during the relaxation. A third, negative-SLA peak occurs shortly after the end of El Niño. This three-peak SLA signal off the Indian east coast is as characteristic of an El Niño as the monotonic SLA signal is for a positive IOD. During combined events, the two peaks that occur during a typical El Niño are seen, and their strength depends on the strength of the two modes and their relative phases. Negative IOD and La Niña events also leave their characteristic signatures. The former is characterized by a single positive SLA peak and the latter by two positive SLA peaks. These signals, however, are weaker in comparison to the negative SLAs seen during positive IOD and El Niño events.

[50] Model solutions show that two forcing processes are important during IOD and ENSO events: equatorial forcing by the reflection of equatorial Kelvin waves at the Sumatra coast as westward propagating Rossby waves (Solutions EQ); and direct forcing by the winds over the interior of the BoB (Solutions INT). Direct forcing is important during a positive IOD and has a considerable impact in southwestern bay, causing positive SLAs in that region. During ENSO, Solution INT is much weaker and the double peak in negative SLAs with relaxation in between the peaks is mainly driven by solution EQ.

[51] Both the observed data and our solutions show that IOD and ENSO signals are not evident along the west coast of India. The distinct patterns associated with both modes give way on the west coast to an indistinct variation in the SLAs. The negative SLAs, which are so clear off the east coast during a positive IOD event, are feeble at Kochi (Cochin), are not seen at all farther poleward. This absence of west coast interannual variability seems to contradict the results of *Clarke and Liu* [1994] and *Shankar and Shetye* [1999], who suggested a coherence between the interannual variability in sea level off the east and west coasts of India. We note, however, that in both studies, the observed anomalies are considerably weaker off the west coast compared to the east coast. Furthermore, there is a difference in the definition of anomalies between these two studies and our work. Here, we define anomalies with respect to the climatological seasonal cycle and examine the change in the seasonal cycle of sea level due to these interannual events; whereas the low-pass filter in *Clarke and Liu* [1994] and *Shankar and Shetye* [1999] would eliminate the seasonal cycle altogether.

[52] In spite of its simplicity, the model captures the observed variability to a remarkable degree (Figures 1 and 2), testifying to the significance of linear dynamics in the NIO. The model simulations are better during the positive IOD events when the wind field over the EIO is more uniform, than during the El Niño events when it exhibits multiple Walker cells [*Ashok et al.*, 2003]. A likely reason for this difference is that the NCEP/NCAR Reanalyses capture more accurately the simpler spatial pattern of the winds during a positive IOD event than they do the more complex spatial patterns of the winds during an El Niño event.

[53] Nevertheless, what emerges from this study is that the impact of IOD and ENSO, the dominant climate modes of the IO, is evident in the BoB, but not in the eastern Arabian Sea. Interannual variability, in the sense of low-frequency, subseasonal periodicities, was shown by *Shankar et al.* [2010] to be similarly weak along the Indian west coast. Therefore, the two studies point to a much weaker interannual variability off the Indian west coast compared to the east coast.

Appendix A

[54] A useful tool for understanding the wind-driven oceanic response is the linear, continuously stratified (LCS) model described here. It has already been used to investigate a variety of Indian-Ocean phenomena [*McCreary et al.*, 1986, 1996, 2007; *Shankar and Shetye*, 1997; *Nethery and Shankar*, 2007]. We present an overview of the model here; additional details can be found elsewhere [*McCreary*, 1980, 1981; *Shankar et al.*, 1996, 2010; *McCreary et al.*, 1996].

[55] The equations of motion of the LCS model are linearized about a state of rest, with a background Brünt-Väisälä frequency, $N_b(z)$, given by the profile of *Moore and*

McCreary [1990]. There is vertical mixing with coefficients of the form $\nu = A/N_b^2$, with $A = 1.3 \times 10^{-4}$ cm^2/s, wind is introduced into the ocean as a body force of the form $Z(z) = \theta(z + H)/H$ where $H = 50$ m, and the ocean bottom is assumed flat with a depth $D = 4000$ m.

[56] Let q be either u, v, or p. Then, q can be written

$$q(x,y,z,t) = \sum_{n=1}^{N} q_n(x,y,t)\psi_n(z), \tag{A1}$$

where the set of functions $\psi_n(z)$ are the vertical (barotropic and baroclinic) modes of the system that satisfy the eigenfunction equation,

$$\left(\frac{\psi_{nz}}{N_b^2}\right)_z = -\frac{1}{c_n^2}\psi_n. \tag{A2}$$

The eigenfunctions are subject to the boundary conditions $\psi_{nz}(0) = \psi_{nz}(-D) = 0$ and are normalized so that $\psi_n(0) = 1$. The eigenvalues c_n are the Kelvin-wave speeds for mode n. The summation in (A1) should extend to ∞, but in practice it must be truncated at a finite value N. In the present study, we use choose $N = 10$, and most of the response is captured by the first two modes. The summation begins at $n = 1$, thereby neglecting the barotropic ($n = 0$) response; as in *McCreary et al.* [1996], the barotropic impact on sea level is weak in comparison to the baroclinic response in our wind-driven solutions.

[57] The set of model equations is

$$\begin{aligned} u_{nt} - fv_n + \frac{1}{\bar{\rho}}p_{nx} &= F_n - \left(\frac{A}{c_n^2}\right)u_n + \nu_h\nabla^2 u_n - \delta u_n, \\ v_{nt} + fu_n + \frac{1}{\bar{\rho}}p_{ny} &= G_n - \left(\frac{A}{c_n^2}\right)v_n + \nu_h\nabla^2 v_n, \\ \frac{1}{c_n^2}p_{nt} + u_{nx} + v_{ny} &= -\left(\frac{A}{c_n^2}\right)p_n - \frac{\delta}{c_n^2}p_n, \end{aligned} \tag{A3}$$

where $F_n = \tau^x Z_n/\mathcal{H}_n$, $G_n = \tau^y Z_n/\mathcal{H}_n$, $\mathcal{H}_n = \int_{-D}^{0}\psi_n^2 dz$, and $Z_n = \int_{-D}^{0} Z(z)\psi_n(z)dz$. The term proportional to $\delta(x, y)$ is a damper in the EEIO ($x > 92.75°$E, $-7.5°$S, $< y < 7.5°$N), which absorbs incoming equatorial Kelvin waves as well as the Rossby waves that reflect from the eastern boundary [*Moore and McCreary*, 1990]. Coefficient δ has a maximum value of $c_n/(1.5\Delta x)$ (where Δx is the zonal grid spacing) in this region, and decreases linearly to zero within 5° of its western edge and within 2° of its northern and southern edges. This damper causes equatorial Kelvin waves to decay rapidly in an e-folding scale of 1.5 Δx and therefore isolates circulations within the Bay from effects due to equatorial forcing.

[58] For most of our solutions, closed, no-slip conditions

$$u_n = v_n = 0 \tag{A4}$$

are applied along continental boundaries, the exceptions being two of our process solutions that use alternate conditions (equations (A5) below). With these closed boundary conditions, the Indonesian passages are always closed so that there is no Indonesian Throughflow in any of our solutions.

[59] Our main run (Solution MR) is the solution obtained using boundary conditions (A4) along all continental boundaries and without the equatorial damper (i.e., $\delta = 0$). To separate the contributions from each of these forcings, we obtain two test solutions (TS). The first solution (Solution TS1) is like MR, but includes the equatorial damper δ. The second solution (Solution TS2) is like MR, except that boundary conditions (A4) are replaced by

$$\begin{aligned} \tilde{u}_n = \boldsymbol{n}\cdot\boldsymbol{v}_n = -\boldsymbol{n}\cdot\boldsymbol{k}\times\frac{\mathbf{F}_n}{f}, \\ \tilde{v}_n = \boldsymbol{k}\times\boldsymbol{n}\cdot\boldsymbol{v}_n = 0, \end{aligned} \tag{A5}$$

where $\boldsymbol{n}$ is a unit vector normal to the boundary, $\boldsymbol{k}$ is a unit vector directed upward, $v_n = (u_n, v_n)$, $\tilde{u}_n$ and $\tilde{v}_n$ are velocity components perpendicular and parallel to the boundary, and $\boldsymbol{F}_n = (F_n, G_n)$. The unit vector $\boldsymbol{n}$ points out of the Bay of Bengal (inshore) along its eastern and northeastern margins, into the bay (offshore) along its northern and western margins, out of the sea (inshore) along the southern boundaries of India and Sri Lanka and along their west coast (eastern Arabian Sea), and into the sea (offshore) along the northern and western boundaries of the Arabian Sea [*Shankar et al.*, 2002]. Condition (5) allows Ekman drift to pass through continental boundaries north of 3.5°N and therefore filters out the effect of alongshore winds.

[60] **Acknowledgments.** We thank S. S. C. Shenoi for valuable suggestions and comments, and Shang-Ping Xie and Yan Du for their help with the covariance analysis. All simulations were carried out on the parallel computer in CSIR-NIO and figures were made using Ferret. Financial support for this work was provided by the Council of Scientific and Industrial Research (CSIR) under the Supra-Institutional Project, by the Indian National Centre for Ocean Information Services (INCOIS) under their INDOMOD project, and by the Ministry of Earth Sciences (MoES), New Delhi under the CTCZ (Continental Tropical Convergence Zone) project. Julian P. McCreary acknowledges the support of the Japan Agency for Marine-Earth Science and Technology (JAMSTEC) through its sponsorship of the International Pacific Research Center. The comments of three anonymous reviewers helped improve this manuscript. This is NIO contribution 5236, SOEST contribution 8757 and IPRC contribution 916.

References

Ashok, K., Z. Guan, and T. Yamagata (2003), A look at the relationship between the ENSO and the Indian Ocean Dipole, *J. Meteorol. Soc. Jpn.*, *81*, 41–56.

Behera, S. A., and T. Yamagata (2003), Influence of the Indian Ocean Dipole on the Southern Oscillation, *J. Meteorol. Soc. Jpn.*, *81*, 169–177.

Berthot, A., C. Pattiaratchi, M. Feng, G. Meyers, Y. Li, and E. Campbell (2005), Understanding the natural variability of currents along the western Australian coastline, *Interim Final Rep.*, pp. 78–87, Strategic Res. Fund for the Mar. Environ., Wembley, W. Austr., Australia.

Busalacchi, A. J., K. Takeruchi, and J. J. OBriene (1983), Interannual variability of the equatorial Pacific—Revisited, *J. Geophys. Res.*, *88*, 7551–7562, doi:10.1029/JC088iC12p07551.

Chambers, D. P., B. D. Tapley, and R. H. Stewart (1999), Anomalous warming in the Indian Ocean coincident with El Niño, *J. Geophys. Res.*, *104*, 3035–3047.

Chelton, D. B., and M. H. Frielich (2005), Scatterometer-based assessment of 10-m wind analyses from the operational ECMWF and NCEP numerical weather prediction models, *Mon. Weather Rev.*, *133*, 409–429.

Clarke, A. J. (2008), *An Introduction to the Dynamics of El Niño and the Southern Oscillation*, Academic, Burlington, Mass.

Clarke, A. J., and X. Liu (1994), Interannual sea level in the northern and eastern Indian Ocean, *J. Phys. Oceanogr.*, *24*, 1224–1235.

Colas, F., X. Capet, J. C. McWilliams, and A. Shchepetkin (2008), 1997–1998 El Niño off Peru: A numerical study, *Prog. Oceanogr.*, *79*, 138–155.

Du, Y., S. P. Xie, G. Huang, and K. M. Hu (2009), Role of air-sea interaction in the long persistence of El Niño–induced north Indian Ocean warming, *J. Clim.*, *22*, 2023–2038.

Ducet, N., P. Y. L. Traon, and G. Reverdin (2000), Global high-resolution mapping of ocean circulation from the combination of T/P and ERS-1/2, *J. Geophys. Res.*, *105*, 19,477–19,498, doi:10.1029/2000JC900063.

Durand, F., F. Papa, A. Rahman, and S. K. Bala (2011), Impact of Ganges-Brahmaputra interannual discharge variations on Bay of Bengal salinity and temperature during 1992–1999 period, *J. Earth Syst. Sci.*, *120*, 859–872.

Han, W., and P. J. Webster (2002), Forcing mechanisms of sea-level interannual variability in the Bay of Bengal, *J. Phys. Oceanogr.*, *23*, 216–239.

Harrison, E. E., and N. K. Larkin (1996), The COADS sea level pressure signal: A near-global El Niño composite and time series view, 1946–1993, *J. Clim.*, *9*, 3205–3255.

Hellerman, S., and M. Rosenstein (1983), Normal monthly wind stress over the World Ocean with error estimates, *J. Phys. Oceanogr.*, *13*, 1093–1104.

Hong, C. C., M. M. Lu, and M. Kanamitsu (2008), Temporal and spatial characteristics of positive and negative Indian Ocean dipole with and without ENSO, *J. Geophys. Res.*, *113*, D08107, doi:10.1029/2007JD009151.

Josey, S. A., E. C. Kent, and P. Taylor (2002), Wind stress forcing of the ocean in the SOC climatology: Comparisons with the NCEP-NCAR, ECMWF, UWM/COADS, and Hellerman and Rosenstein datasets, *J. Phys. Oceanogr.*, *32*, 1993–2019.

Kalnay, E., et al. (1996), The NCEP/NCAR 40-year reanalysis project, *Bull. Am. Meterol. Soc.*, *77*, 437–471.

Klein, S. A., B. J. Soden, and N. C. Lau (1999), Remote sea surface temperature variations during ENSO: Evidence for tropical atmospheric bridge, *J. Clim.*, *12*, 917–932.

McCreary, J. P. (1980), Modelling wind-driven ocean circulation, *Tech. Rep. 80*, 64 pp., Univ. of Hawaii at Manoa, Honolulu.

McCreary, J. P. (1981), A linear stratified ocean model of the equatorial undercurrent, *Philos. Trans. R. Soc. London*, *298*, 603–635.

McCreary, J. P., S. R. Shetye, and P. K. Kundu (1986), Thermohaline forcing of eastern boundary currents: With application to the circulation off the west coast of Australia, *J. Mar. Res.*, *44*, 71–92.

McCreary, J. P., P. K. Kundu, and R. L. Molinary (1993), A numerical investigation of the dynamics, thermodynamics and mixed layer processes in the Indian Ocean, *Prog. Oceanogr.*, *31*, 181–224.

McCreary, J. P., W. Han, D. Shankar, and S. R. Shetye (1996), Dynamics of the East India Coastal Current: 2. Numerical solutions, *J. Geophys. Res.*, *101*, 13,993–14,010.

McCreary, J. P., T. Miyama, R. Furue, T. Jensen, H. W. Kang, B. Bang, and T. Qu (2007), Interactions between the Indonesian Throughflow and circulations in the Indian and Pacific Oceans, *Prog. Oceanogr.*, *75*, 70–114.

Moore, D. W., and J. P. McCreary (1990), Excitation of intermediate-frequency equatorial waves at a western boundary: With application to observations from the western Indian Ocean, *J. Geophys. Res.*, *96*, 2515–2534.

Murtugudde, R., J. Busalacchi, and J. Beauchamp (1998), Seasonal to interannual effects of the Indonesian Throughflow on the tropical Indo-Pacific basin, *J. Geophys. Res.*, *103*, 21,425–21,441.

Murtugudde, R., J. P. McCreary, and J. Busalacchi (2000), Oceanic processes associated with anomalous events in the Indian Ocean with relevance to 1997–1998, *J. Geophys. Res.*, *105*, 3295–3306.

Nethery, D., and D. Shankar (2007), Vertical propagation of baroclinic Kelvin waves along the west coast of India, *J. Earth Syst. Sci.*, *116*, 331–339.

Philander, S. G. H. (1990), *El Nino, La Niña and the Southern Oscillation*, Academic, San Diego, Calif.

Ponte, R. M. (1993), Variability in a homogeneous global ocean forced by barometric pressure, *Dyn. Atmos. Oceans*, *18*, 209–234.

Potemra, J. T., M. E. Luther, and J. J. O'Brien (1991), The seasonal circulation of the upper ocean in the Bay of Bengal, *J. Geophys. Res.*, *96*, 12,667–12,683.

Rao, A. S., S. K. Behera, Y. Masumoto, and T. Yamagata (2002a), Interannual subsurface variability in the tropical Indian Ocean with a special emphasis on the Indian Ocean Dipole, *Deep Sea Res., Part II*, *49*, 1549–1572.

Rao, A. S., V. V. Gopalakrishna, S. R. Shetye, and T. Yamagata (2002b), Why were cool SST anomalies absent in the Bay of Bengal during the 1997 Indian Ocean Dipole Event?, *Geophys. Res. Lett.*, *29*(11), 1555, doi:10.1029/2001GL014645.

Reverdin, G. (1985), Convergence in the equatorial surface jets of the Indian Ocean, *J. Geophys. Res.*, *90*, 11,741–11,750.

Saji, N. H., and T. Yamagata (2003), Structure of SST and surface wind variability during Indian Ocean Dipole Mode events: COADS observations, *J. Clim.*, *16*, 2735–2751.

Saji, N. H., B. N. Goswami, P. N. Vinayachandran, and T. Yamagata (1999), A dipole mode in the tropical Indian Ocean, *Nature*, *401*, 360–363.

Saji, N. H., T. Ambrizzi, and S. E. T. Ferraz (2005), Indian Ocean Dipole mode events and austral surface air temperature anomalies, *Dyn. Atmos. Oceans*, *39*, 85–101.

Schott, F. A., S. P. Xie, and J. P. McCreary (2009), Indian Ocean circulation and climate variability, *Rev. Geophys.*, *47*, RG1002, doi:10.1029/2007RG000245.

Shankar, D. (1998), Low-frequency variability of sea level along the coast of India, PhD thesis, Goa Univ., Goa, India.

Shankar, D., and S. R. Shetye (1997), On the dynamics of the Lakshadweep high and low in the southeastern Arabian Sea, *J. Geophys. Res.*, *102*, 12,551–12,562.

Shankar, D., and S. R. Shetye (1999), Are interdecadal sea level changes along the Indian coast influenced by variability of monsoon rainfall?, *J. Geophys. Res.*, *104*, 26,031–26,042.

Shankar, D., J. P. McCreary, W. Han, and S. R. Shetye (1996), Dynamics of the East India Coastal Current: 1. Analytic solutions forced by interior Ekman pumping and local alongshore winds, *J. Geophys. Res.*, *101*, 13,975–13,991.

Shankar, D., P. Vinayachandran, and A. S. Unnikrishnan (2002), The monsoon currents in the north Indian Ocean, *Prog. Oceanogr.*, *52*, 63–120.

Shankar, D., S. G. Aparna, J. P. McCreary, I. Suresh, S. Neetu, F. Durand, and S. S. C. Shenoi (2010), Minima of interannual sea-level variability in the Indian Ocean, *Prog. Oceanogr.*, *84*, 225–241.

Singh, O. P. (2002), Interannual variability and predictability of sea level along the Indian Coast, *Theor. Appl. Climatol.*, *72*, 11–28.

Srinivas, K., P. K. D. Kumar, and C. Revichandran (2005), ENSO signature in the sea level along the coastline of the Indian subcontinent, *Indian J. Mar. Sci.*, *34*, 225–236.

Strub, P. T., and C. James (2002), The 1997–1998 oceanic El Niño signal along the southeast and northeast Pacific boundaries—An altimetric view, *Prog. Oceanogr.*, *54*, 439–458.

Thompson, B., C. Gnanaseelan, and P. S. Salvekar (2006), Variability in the Indian Ocean circulation and salinity and its impact on SST anomalies during dipole events, *J. Mar. Res.*, *64*, 853–880.

Tozuka, T., J. J. Luo, S. Masson, and T. Yamagata (2008), Tropical Indian Ocean variability revealed by self-organizing maps, *Clim. Dyn.*, *31*, 331–343, doi:10.1007/s00382-007-0356-4.

Trenberth, K. E. (1997), The definition of El Niño, *Bull. Am. Meteorol. Soc.*, *78*, 2771–2777.

Vinayachandran, P. N., and S. Mathew (2003), Phytoplankton bloom in the Bay of Bengal during the northeast monsoon and its intensification by cyclones, *Geophys. Res. Lett.*, *30*(11), 1572, doi:10.1029/2002GL016717.

Vinayachandran, P. N., and T. Yamagata (1998), Monsoon response of the sea around Sri Lanka: Generation of thermal domes and anticyclonic vortices, *J. Phys. Oceanogr.*, *28*, 1946–1960.

Vinayachandran, P. N., Y. Masumoto, T. Mikawa, and T. Yamagata (2002), Indian Ocean dipole mode events in an ocean general circulation model, *Deep Sea Res., Part II*, *49*, 1573–1596.

Vinayachandran, P. N., P. A. Francis, and S. A. Rao (2009), Indian Ocean Dipole: Processes and impacts, in *Current Trends in Science*, pp. 569–589, Indian Acad. of Sci., Bangalore, India.

Webster, P. J., A. M. Moore, J. P. Loschnigg, and R. R. Leben (1999), Coupled ocean-atmosphere dynamics in the Indian Ocean during 1997–98, *Nature*, *401*, 356–360.

Wyrtki, K. (1971), *Oceanographic Atlas of the International Indian Ocean Expedition*, 531 pp., Natl. Sci. Found., Washington, D. C.

Xie, S. P., K. Hu, J. Hafner, H. Tokinaga, Y. Du, G. Huang, and T. Sampe (2009), Indian Ocean capacitor effect on Indo-Western Pacific climate during the summer following El Niño, *J. Clim.*, *22*, 730–747.

Yu, L. (2003), Variability of the depth of the 20°C isotherm along 6°N in the Bay of Bengal: Its response to remote and local forcing and its relation to satellite SSH variability, *Deep Sea Res., Part II*, *50*, 2285–2304.